Establishing the excitation field in tip-enhanced Raman spectroscopy to study nanostructures within two-dimensional systems

To cite this article: Hudson Miranda *et al* 2023 *2D Mater.* **10** 015002

2D Materials

PAPER

RECEIVED
27 June 2022

REVISED
3 October 2022

ACCEPTED FOR PUBLICATION
7 October 2022

PUBLISHED
20 October 2022

Establishing the excitation field in tip-enhanced Raman spectroscopy to study nanostructures within two-dimensional systems

Hudson Miranda[1], Vitor Monken[1], João Luiz E Campos[1], Thiago L Vasconcelos[2], Cassiano Rabelo[1], Bráulio S Archanjo[2], Clara M Almeida[2], Sebastian Grieger[3], Claudia Backes[3,4], Ado Jorio[1] and Luiz Gustavo Cançado[1,*]

[1] Departamento de Física, Universidade Federal de Minas Gerais, Belo Horizonte, Minas Gerais 30123-970, Brazil
[2] Divisão de Metrologia de Materiais, Instituto Nacional de Metrologia, Qualidade e Tecnologia, Duque de Caxias, Rio de Janeiro 25250-020, Brazil
[3] Institute for Physical Chemistry, Ruprecht-Karls-Universität Heidelberg, Im Neuenheimer Feld 253, 69120 Heidelberg, Germany
[4] Current address: Physical Chemistry of Nanomaterials, University of Kassel, Heinrich-Plett-Str.40, D-34132 Kassel, Germany.
[*] Author to whom any correspondence should be addressed.

E-mail: cancado@fisica.ufmg.br

Keywords: tip-enhanced Raman spectroscopy, twisted bilayer graphene, graphene edges, excitation field

Supplementary material for this article is available online

Abstract

The optical field generated by a nanoplasmonic probe is revealed in tip-enhanced Raman spectroscopy (TERS) experiments. The TERS intensity profile of nano-objects smaller than the probe's apex has a donut-like shape which resembles the magnitude of the field generated by a point-dipole source, being well described by the Dyadic Green's function. Having prior knowledge on the excitation field generated by the TERS probe, we measured the width of shear solitons caused by lattice reconstruction in low-angle twisted bilayer graphene, a prominent platform for twistronics, and the extend of defect-induced light emission from graphene edges.

1. Introduction

Accurate imaging of nanostructures requires deep understanding of the probe and how it interacts with the measurand. In nano-optics techniques [1], such as tip-enhanced Raman spectroscopy (TERS) [2–8], the electric field generated by a nanoantenna is mostly directed along the axis of the probe and, for this reason, the transversal components of the field are generally underlooked. This approximation can be seriously misleading when studying surfaces or two-dimensional systems, where the material is actually covering the plane transverse to the probe axis [9].

It has been shown that the gradient of the electric field plays an important role in terms of spatial resolution [10] and non-linear effects in TERS [3, 11–14]. A comprehensive understanding of these findings demand accurate description of the spatial distribution of the optical field, which is routinely attempted by solving Maxwell's equations through numerical calculations such as in the finite element method [3, 10, 13–15]. Here we establish the donut-like shape of the transversal component of the optical field generated by a TERS probe by measuring graphene nanosheets smaller than the near-field mode distribution [16]. The fields are accurately described by the Dyadic Green's function with a point-dipole source. With the proper description of the excitation, the spatial distribution for defect-induced light emission from the edges of the material [17] is directly probed, and the actual width of a domain-wall appearing in a reconstructed twistronic system [18] is measured, the later showing consistency with transmission electron microscopy observation [19]. With this development the nano-optics at ambient conditions can be utilized for more in depth studies of nanostructures.

2. Results and discussion

Figure 1(a) shows a TERS image of graphene flakes dispersed on a glass coverslip, where the color scale represents the spectral intensity. This specific sample was chosen for exhibiting crystalline graphene

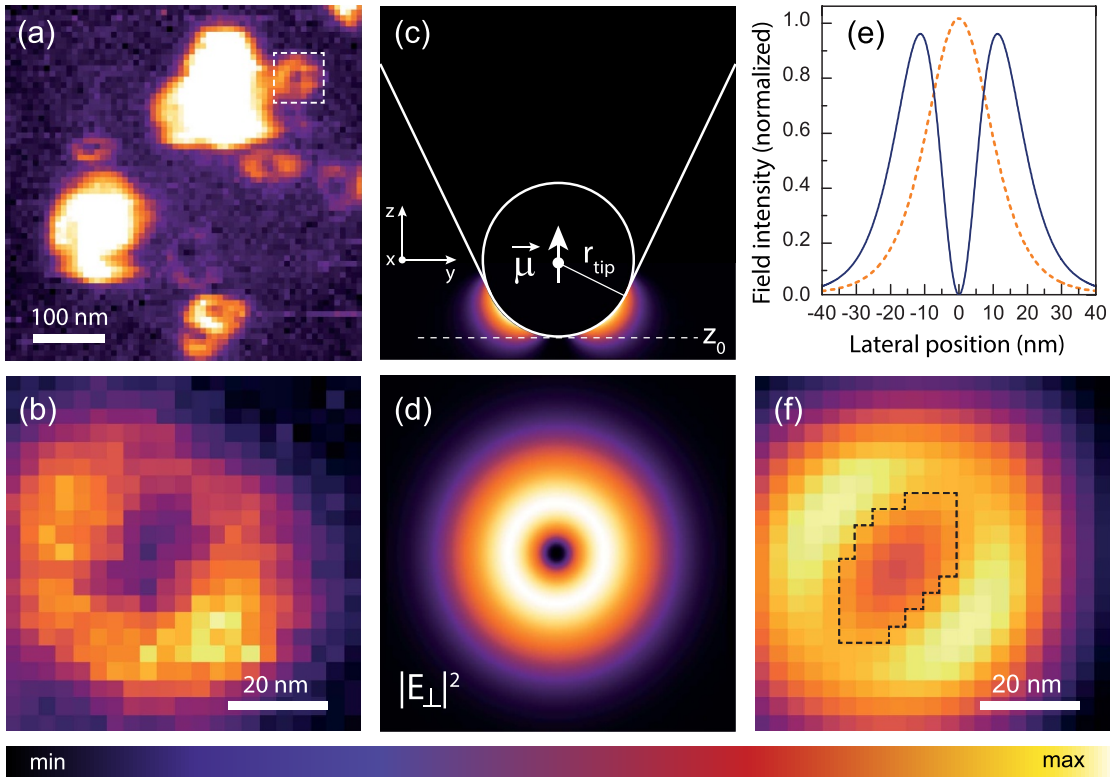

Figure 1. (a) TERS image of graphene nanoflakes, where the color scale represents the intensity (integrated area) of the disorder-induced D band, centered at ≈1350 cm^{-1} [20]. (b) D band's intensity image of the area surrounded by the white-dashed rectangle in (a). (c) Spatial map over the *yz* plane of the amplitude squared of the transversal component $\mathbf{E}_\perp$ of the field generated by a point-dipole positioned at the center of a sphere with radius r_{tip}. (d) Spatial distribution of $|\mathbf{E}_\perp|^2$ over the *xy*-plane located at a vertical distance z_0 from the apex of the nanoplasmonic tip. For the plots in (c) and (d) we considered $r_{tip} = 15$ nm, $z_0 = 5$ nm, and excitation laser wavelength $\lambda = 632.8$ nm, all consistent with the experimental conditions. (e) Line profiles of square amplitude of the longitudinal $\mathbf{E}_z$ and transversal $\mathbf{E}_\perp$ components of the TERS field (dotted orange and solid blue lines, respectively), with $|\mathbf{E}_\perp|^2$ multiplied by 100×. (f) Reconstruction of the TERS intensity shown in (b), obtained by numerical integration of equation (1) (see section 4.3), considering a nanoflake whose boundaries are illustrated by the dashed-contour line, as obtained by a two-dimensional fit of the experimental TERS intensity map (see section 4.6).

nanosheets (details on sample preparation [21] and experimental apparatus [22, 23] are presented in sections 4.1 and 4.2). Around typical graphite nanoflakes with lateral sizes >100 nm, a few smaller donut-shaped spectral responses are seen. Figure 1(b) highlights one of these donuts by showing a magnified image of the area surrounded by the withe-dashed square in figure 1(a). All these donut-shaped features originate from graphene nanosheets smaller than ten(s) of nanometers and the nano-donuts are actually the outcome from a spatial convolution of the radiation field from the TERS tip with the nanosheet (see corresponding atomic force microscopy image and representative Raman spectrum in supplementary figures S1 and S2, respectively).

To gather information on the shape of these tiny graphene nanosheets, it is necessary to deconvolve the exciting optical field generated by the TERS tip within the sample plane, because graphene responds optically only to in-plane polarized fields [15]. The excitation can then be modeled as the transversal field $\mathbf{E}_\perp$ of a point-dipole positioned at the center of a sphere with radius r_{tip}. This sphere represents the rounded apex of the tip, as illustrated in figure 1(c), where the colors give the spatial distribution of $|\mathbf{E}_\perp|^2$, as described by the Dyadic Green's function (see section 4.3). Figure 1(d) shows the spatial distribution of $|\mathbf{E}_\perp|^2$ over the sample plane (perpendicular to the probe axis) located at a vertical distance z_0 from the apex of the nanoplasmonic tip, where z_0 represents the typical tip-sample working separation. This image provides a hint for understanding the donut shape of the spectral response from the nanosheets observed in the TERS measurement in figures 1(a) and (b). The blue solid line in figure 1(e) shows $|\mathbf{E}_\perp|^2$ ×100 along a line profile crossing the center of the donut. For comparison, the same graphics shows the plot of the square amplitude of the longitudinal component of the field generated by the tip, $|\mathbf{E}_z|^2$. Despite being two-orders of magnitude stronger than $\mathbf{E}_\perp$, the $\mathbf{E}_z$ does not excite the two-dimensional graphene nanosheets [15] and $\mathbf{E}_\perp$ fully dominates the TERS response.

Different from what is seen in figure 1(d), the experimentally obtained donut shape in figure 1(b) is not circularly symmetric with a null response at the very center, and these spatial differences reflect the actual sample's geometry. The theoretical

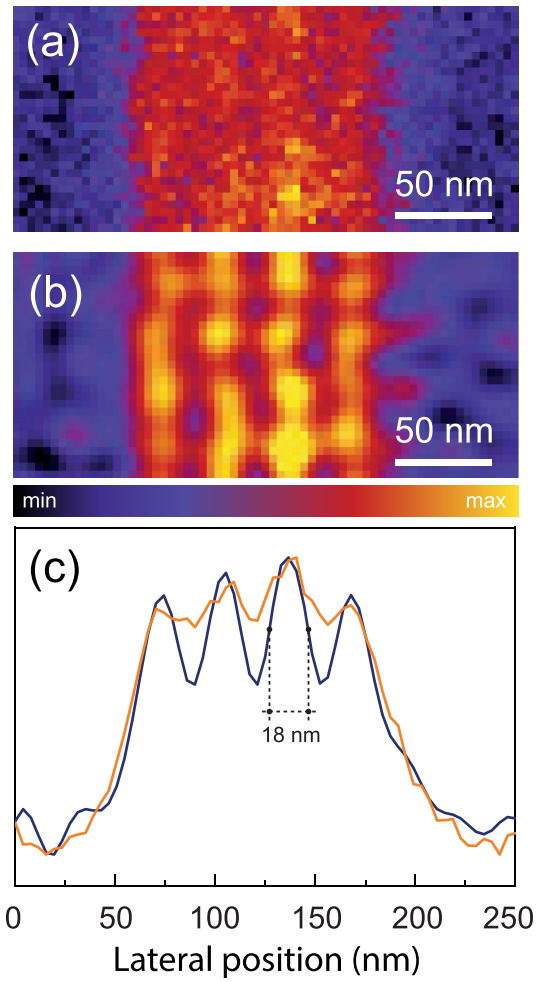

Figure 2. (a) TERS map of the D band intensity over a row of defective stripes drawn with a He-focused ion beam (details in section 4.1). (b) The same image as in (a) after deconvolution of the donut-shaped transversal field. A tip radius of 12 nm was considered, as measured by scanning electron microscopy (see figure S3 in the supplementary material available). (c) Average intensity profile of the original (orange) and deconvolved (dark blue) TERS images.

reconstruction of the TERS intensity is shown in figure 1(f), considering the convolution of the excitation field (figure 1(d)) and the nanosheet, whose shape is highlighted by the dashed-contour line, as obtained by a two-dimensional fit of the entire TERS intensity map in figure 1(b) (see details on the reconstruction procedure in section 4.4). Notice that when the sample is centered right below the tip (as drawn in figure 1(f)), the intensity exhibits a minimum, and the scattering maxima happens when the sample is scanned out of center through the nano-donut illumination mode.

The knowledge of the excitation field can also be utilized to improve image resolution, as exemplified in figure 2(a), in which a row of defective stripes produced by He-focused ion beam (details on sample preparation are presented in section 4.1). The bare image shown in figure 2(a) stands for the D band's TERS intensity, which is stronger at the defective stripes. Figure 2(b) shows the same image deconvolved from the donut-shaped transversal field. The details on the deconvolution process are provided in section 4.5.

Figure 2(c) shows the average intensity profiles of the original (orange) and deconvolved (blue) TERS images. The plot demonstrates how the visibility of the stripes is significantly improved in the treated image. Such improvement evidences the fact that the lines generated by the He-focused ion beam are not as continuous as one would expect, but they rather exhibit a set of spots where the ion millings were more effective. A previous atomic force microscopy (AFM) study of graphene processed by He-focused ion beam using similar ion doses and patterning strategies was presented in [24]. Besides, we performed an AFM analysis of the sample presented in figure 2(c), and the result is shown in supplementary figure S4. The AFM height-profile of the patterned area (panel S4(b)) reveals that the defective lines have an average width of 17 nm. This is similar to the width obtained from the intensity-profile analysis of the deconvoluted TERS data, which is approximately 18 nm, as shown in figure 2(c).

It is necessary to stress that, in extreme conditions, such as sub-nanometer tip radius and ST working distance operating at ultra-high vacuum [2, 6, 7], other parameters in image reconstruction will prevail [3, 10–14], while the picture shown here applies to broadly-accessible ambient condition experiments.

The ability to improve image resolution allows us to accurately measure and extract higher information levels. For example, recent TERS study of twisted bilayer graphene (tBLG) shows that the domain walls have Raman signatures distinct from the neighboring AB or BA stacking regions [8]. We can now investigate the width of these domain walls observed between bilayer graphene regions with a stacking mismatch [19, 25–28]. Recent TERS study of tBLG shows that the strain solitons have Raman signatures distinct from the regular AB or BA stacking regions [8]. While the bond-stretching G band (at $\approx$1580 cm^{-1}) presents an upper shifted satellite peak originated from localized phonon states, the well-known four-Lorentzian shape of the 2D band observed in the Bernal stacked bilayer graphene assumes a more symmetric shape, as a consequence of the changes in the electronic structure due to local strain [8]. Besides, the 2D band presents a lower intensity over a strain soliton if compared to the Bernal stacked regions.

Figure 3(a) shows a TERS map of the 2D band's intensity. The darker segment indicates the presence of a domain wall [8]. Theoretical calculations indicate that the lower intensity of the 2D band along the strain soliton is related to a lower joint density of electronic states for optical transitions near 1.96 eV, which is the photon energy of the HeNe excitation laser used in the experiment (wavelength of 632.8 nm) [8]. Figure 3(b) shows the drop in intensity

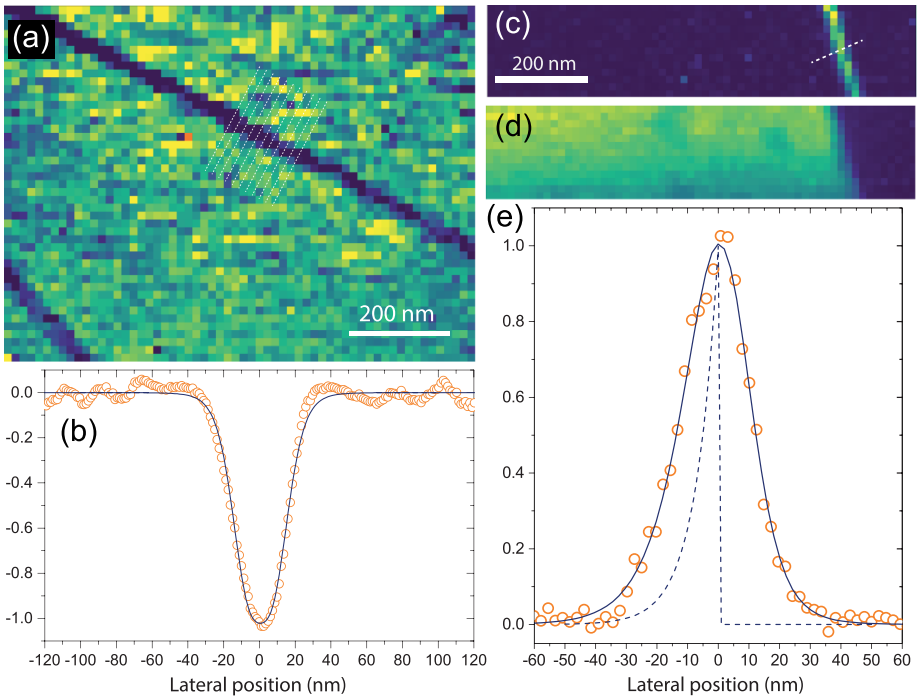

Figure 3. (a) TERS map of the 2D band's intensity in reconstructed twisted bilayer graphene [8]. The darker segment indicates the presence of domain walls in the connection of AB and BA stacked regions. Reproduced from [8], with permission from Springer Nature. (b) Intensity drop profile of the 2D band's intensity when crossing a domain wall, obtained by averaging ten line-profiles indicated by the dash lines in panel (a). The solid line is the fit of the experimental data (open circles), which determines $\ell_{SP} = 12.3 \pm 2.0$ nm for $r_{tip} = 12.0 \pm 0.6$ nm. (c) and (d) TERS intensity maps of a graphene edge. Both plots were extracted from the same hyperspectral map, and represent the integrated areas of the first-order defect-induced D band ($\approx$1350 cm^{-1}) and the second-order Raman-allowed 2D band ($\approx$2700 cm^{-1}), respectively. (e) TERS D band's intensity profile extracted along the dashed line in panel (c). The dark solid line is the fit to the experimental data obtained by numerical integration of equation (1), considering the Raman susceptibility (dashed line) according to equation (4) in section 4.6. The fit determines a coherence length of $\ell_D = 7.8 \pm 3.2$ nm for $r_{tip} = 17.3 \pm 7.0$ nm.

of the 2D band's when crossing a domain wall, obtained here by averaging ten line-profiles indicated by the dash lines in figure 3(a). Assuming consistently that the 2D band's susceptibility has a Gaussian shape with full-width at half-maximum ℓ_{SP}, the fit of the experimental data (solid line) gives $\ell_{SP} = 12.3 \pm 2.0$ nm, in excellent agreement with results obtained with scanning tunneling microscopy [25]. These graphene domain walls are classified into two types, namely shear and tensile solitons [19, 28]. Based on previous transmission electron microscopy analysis [19] and theoretical calculations [26], we conclude that the strain soliton shown in figure 3(a) is of the tensile type.

We also apply our developed technique to study the behavior of electrons and phonons at the border of two-dimensional systems, important for their optical, electronic and thermal properties when designed as transport channels. Due to momentum conservation, first-order Raman scattering is limited to phonons with wavevector $q = 0$. In graphene, the breakdown of momentum conservation due to defects in the crystalline network generates the defect-induced Raman D band, associated with phonons with $q \neq 0$ [29], and this phenomenon has been broadly utilized for quality control or graphene related systems [20]. Consequently, the D band can also be observed at the border of graphene [17]. Figures 3(c) and (d) show TERS intensity maps of a graphene edge. Both panels were extracted from the same hyperspectral map, and represent the integrated areas of the first-order defect-induced D band and of the second-order Raman-allowed 2D band (with $q - q = 0$, momentum is conserved), respectively [20].

The localization ℓ_D of the D band near the edge, relying on the coherence length of photo-excited electrons involved in the phonon scattering process [30], has been a theme of debate. Previous indirect micro-Raman experimental results indicate $\ell_D = 4 \pm 1$ nm [30–32]. By fitting the D band intensity profile across the edge (see figure 3(e) and related discussion in section 4.6) we found $\ell_D = 7.8 \pm 3.2$ nm. The value of ℓ_D is in agreement with previous microscopic studies [30–32], but determined here directly with higher accuracy.

3. Conclusions

We have demonstrated here that a rather simple analytical model, based on a single point-dipole's field, provides accurate description of the nano-Raman system point spread function, enabling to extract structural information from nano-sized systems with unprecedented resolutions in nano-optics

measurements, in ambient conditions. This finding allowed us to directly probe the nm-decay of phonon-mediated inelastic light emission from graphene borders and to accurately establish the width of stacking dependent domain wall in twisted bi-layers. We also evidenced unexpected modulations in He-FIB milling. These might be significant achievements for understating and designing mesoscopic devices where nanostructures within two-dimensional systems play a role.

4. Materials and methods

4.1. Experimental details

A ORION NanoFab microscope (Zeiss) working with 30 kV was used to draw the helium-ion induced defective lines on a mechanically exfoliated single-layer graphene sample, as shown in figure 2. The pattern was produced with a low ion dose of 1×10^{16} ion cm^{-2} to avoid intense erosion regions. The pattern is composed by an array of lines formed by a series of spots separated by 1 nm and with 50 μs of dwell time. The separation distance between the parallel stripes is 33 nm. To avoid sample damage, the flood gun was used with lower source voltage (1 V) than conventionally used (1.5 V), with the sample tilted by 15 ° to fine-tune the focus and astigmatism.

The sample in figure 3(a) is a twisted bilayer graphene and the data was obtained from [8], available at https://doi.org/10.5281/zenodo.4313869. The sample in figures 3(c) and (d) is a monolayer graphene produced by mechanical exfoliation of highly-oriented pyrolytic graphite.

All TERS images were obtained with a plasmon tunable pyramid tip [22] coupled to the TERS instrument described in [23].

4.2. Graphene nanosheets preparation and deposition

About 2.4 g of graphite (Sigma Aldrich 332461) were immersed in 80 ml of aqueous sodium cholate solution (8 g l^{-1}) in a round bottom flask and subjected to sonication in a hot spot of a Branson CPX3800 sonication bath. After a sonication time of 1 h, the dispersion was centrifuged at 3860 g for 2 h at 10 °C (using a Hettich Mikro 220 R centrifuge equipped with a fixed-angle rotor 1016) and the impurity-rich supernatant discarded. The sediment was collected in fresh aqueous sodium cholate solution (2 g l^{-1}) for a second exfoliation step with a sonication time of 5 h. During the bath sonication, the bath water was replaced every 60 min with new water to avoid overheating. From our experience, a two-step sonication procedure removes (ionic) impurities in the bulk material resulting in improved exfoliation and colloidal stability in surfactant solutions [33].

To isolate small and thin nanosheets, centrifugation was performed subsequently at 100 g, 400 g, 1000 g (2 h, 10 °C, in a Hettich Mikro 220 R centrifuge equipped with a fixed-angle rotor 1016) and 5000 g (2 h, 10 °C in a Beckman Coulter Avanti XP centrifuge with a JA25.50 fixed angle rotor) and the sediments containing larger/thicker sheets were discarded. The supernatant after the fourth step was centrifuged at 10 000 g (2 h, 10 °C in a Beckman Coulter Avanti XP centrifuge with a JA25.50 fixed angle rotor) and the sediment redispersed in 0.1 g l^{-1} aqueous sodium cholate solution. This last centrifugation step was performed to remove impurities in the supernatant.

For deposition, the dispersion was diluted with deionized (D.I.) water to an optical density of $\simeq 0.3$ cm^{-1} in the plateau region of the optical extinction spectra at >700 nm and deposited on borosilicate glass cover slips (Knittel, VD12424Y1A.01) coated with 3-Aminopropyl triethoxysilane (APTS). To this end, the substrate was first immersed in the APTS solution (2 ml APTS diluted in 78 ml D.I water) for 15 min. This will form a monolayer covering the entire substrate. Subsequently, the substrate was removed, washed repeatedly with D.I water, and dried under a stream of nitrogen. Then, the nanomaterial dispersion was dropped onto the substrate and held for $\simeq$ 20 s. Subsequently, the drop was discarded (e.g. blown off with pressurized nitrogen) and the sample washed with $\simeq$ 5 ml D.I. water.

To assess the average, bulk properties of the liquid-phase exfoliation (LPE) graphene, the dispersion was subjected to optical extinction spectroscopy (supplementary figure S5(a)—Agilent Cary 6000i UV–Vis-NIR spectro-photometer, 200–1000 nm, 0.5 nm spectral resolution, 0.1 s integration time in a fused quartz cuvette with 0.4 cm path length). Further, a drop of concentrated dispersion was deposited on Si/SiO_2 and (average) Raman spectra were acquired on randomly restacked nanosheets in air under ambient conditions (supplementary figure S5(b)—Renishaw InVia-Reflex confocal Raman microscope, 532 nm excitation laser, 50× long working distance objective lens in streamline mode, 2400 l mm^{-1} grating with 1% of the laser power of 1.23 μW and 10 s integration time, three individual spectra are averaged). In both cases, the characteristic spectral profiles consistent with few-layer graphene was observed [34]. Further, AFM was performed (supplementary figures S5(c) and (d)) showing 2D platelets with characteristic shape and sharp edges alongside small features that cannot be resolved clearly with AFM in ambient conditions.

It might be surprising that such small nanosheets (<15–20 nm) are observed in the TERS measurements shown in figures 1(a) and (b). However, it should be noted that no peculiarities were obvious from the characterization of the nanosheets in dispersion. This is likely a result of the polydispersity of the sample and that larger/

thicker nanosheets with higher mass (such as the ones with a characteristic platelet shape in AFM) dominate the average spectral response. Note that the very small nanosheets can hardly be identified as graphene and might therefore be easily overlooked in routine characterization. Nonetheless, indications that quantum dot like graphene is produced by sonication-assisted LPE can be found in literature. To isolate such small structures and increase their production yield, typically it is required to perform some additional treatments, for example with chemicals such as alkaline solutions [35, 36] or by pulsed laser ablation [37]. However, they have also been observed after bath sonication of nanographite in N-methyl-2-pyrrolidone [38]. It is thus plausible that they are present as minority fraction (by mass) in common LPE processes.

4.3. TERS intensity calculation

In TERS, the tip-radiation interaction can occur with the excitation field, the scattered field, or both. These three possible events are denominated by tip-sample (ST), sample-tip (TS), and tip-sample-tip (TST), respectively [39]. As for operators, the notation reads backwards. In ST, the focused incident laser field interacts first with the tip, and the sample is then excited by the locally-enhanced secondary field generated by the tip. The TS works in the other way around: the sample is excited by the incident focused laser beam, and the tip interacts with the scattered Raman field. As clearly indicated by the notion, both incident and scattered fields interact with the tip in the TST process. Considering the TS, ST and TST sequences, the TERS intensity amplified by the nanoplasmonic tip positioned at $\mathbf{r} = (x, y, z_0 + r_{\mathrm{tip}})$ can be spatially mapped as [39]

$$I(\mathbf{r}) = \frac{\omega_s^4 E_0^2}{\varepsilon_0^2 c^4} \left\{ \frac{4}{3} A^2 \int \left[\sum_{i=x,y} G_{iz}^*(\mathbf{r}', \mathbf{r}) G_{iz}(\mathbf{r}', \mathbf{r}) \right] \times \chi_\gamma^2(\mathbf{r}')\, d^2 r' + A^4 \int \left[\sum_{i=x,y} G_{iz}^*(\mathbf{r}', \mathbf{r}) G_{iz}(\mathbf{r}', \mathbf{r}) \right]^2 \times \chi_\gamma^4(\mathbf{r}')\, d^2 r' \right\} \quad (1)$$

where the integral sums run over the entire sample plane, scanning the position $\mathbf{r}' = (x', y', 0)$. In equation (1), ω_s is the frequency of the scattered field, E_0 is the amplitude of the incident laser field, ε_0 and c are the permittivity and speed of light in free space, respectively; $\chi_\gamma(\mathbf{r}')$ provides the spatial distribution of the Raman response associated with a specific vibrational mode γ, and A is a fitting parameter which accounts for the volume and enhancement factor of the nanoplasmonic structure. $G_{iz}(\mathbf{r}', \mathbf{r})$ is the iz component of the Dyadic Green's function tensor with $i \in \{x, y\}$, whose square modulus is explicitly described as

$$G_{iz}^*(\mathbf{r}', \mathbf{r}) G_{iz}(\mathbf{r}', \mathbf{r}) = \frac{(i - i')^2 z^2}{(4\pi)^2 k^4} \left(\frac{9 + 3k^2 |\mathbf{r} - \mathbf{r}'|^2 + k^4 |\mathbf{r} - \mathbf{r}'|^4}{|\mathbf{r} - \mathbf{r}'|^{10}} \right), \quad (2)$$

where k is the wavevector of the radiation field. Unlike in [39], the Green's function component (2) accounts not only for the near field, but also for the intermediate and far field components. It should also be noted that, for simplicity, equation (1) does not account for interference effects. Coherence-related aspects of the Raman field are important for understanding different levels of enhancement for Raman modes with distinct symmetries [39], which is out of scope of this work.

4.4. TERS reconstruction process

The reconstruction of the graphene nanoflake presented in figure 1(f) was performed through numeric evaluation of equation (2). The spatial distribution of the material's Raman response χ_γ, used to map the actual shape of the nanoflake, was modeled as a parameterized homogeneous ellipse. The free parameters involved were the tip's response A, the tip's radius, and the ellipse's size, eccentricity, rotation, and central position. The fitting procedure was performed over the experimental data shown in figure 1(b). The differential evolution algorithm, as implemented by the LMFIT library [40], was chosen to assure convergence. The dotted line shown in figure 1(f) represents the resulting ellipse that better reproduces the actual shape of the nanoflake.

4.5. Deconvolution of the transversal field from the Raman susceptibility

To deconvolve the donut-shaped transversal field from the D band's intensity map shown in figure 2(a), we applied the well-known Richardson–Lucy algorithm [41, 42], as implemented by the scikit-image package for SciPy [43]. Since the TERS signal is given by a convolution of material's Raman response χ_γ with the tip's dipole field, the deconvolution algorithm consists of finding the best approximation, iteratively, of the original signal

$$\hat{u}^{(t+1)} = \hat{u}^{(t)} \cdot \left(\frac{\chi_\gamma}{\hat{u}^{(t)} \otimes P} \otimes P^* \right), \quad (3)$$

where P and P^* are the dipole's field and its mirrored field, respectively, and $\otimes$ indicates a 2D convolution.

To avoid artifacts in the resulting image, the raw D band intensity map was previously filtered using a low-pass filter defined in the frequency domain, as implemented by Gwyddion 2.61 *2D FFT Filtering Tool* [44]. The cut-off spatial frequency was set to

33 μm^{-1}, to preserve the features of interest. This frequency was chosen in an interactive fashion, reducing the cut-off frequency while preserving the lack of correlation in the residual noise from the filtering process.

4.6. Fitting the Raman susceptibility function

In order to fit the 2D band drop in figure 3(b), as well as the D intensity profile presented in figure 3(e), custom objective functions were elaborated and submitted to a least-squares minimization algorithm. The objective functions were designed to simulate the intensity profile of a given Raman feature, namely by discretely convoluting the Dyadic Green's function, as presented in equation (2), with the specific susceptibility response. Although the convolution's operands are two-dimensional, the convolution was conducted in one dimension, to properly resemble an actual scanning procedure of the TERS measurement. These objective functions were used, along with the experimental data, as inputs of a non-linear least squares optimization algorithm, as implemented by the SciPy [45] library in order to estimate probe and sample parameters. Additionally, the two-dimensional fitting process for the nano-donut in figure 1(b) was conducted using the differential evolution as implemented by the LMFit library [46] using Python. This was done to enable convergence with the increased number of free parameters, namely seven, and the relatively small number of observations, in this case, 441.

For the D band's TERS intensity near the edge of a graphene flake, as in figure 3(e), we considered an exponentially decaying Raman susceptibility:

$$\chi_D(x) = \begin{cases} \exp[-(x - x_e)/\ell_D], & x \leqslant x_e \\ 0, & x > x_e \end{cases}, \quad (4)$$

where x is the spatial coordinate along the direction perpendicular to the edge, with x_e marking its position.

Data availability statement

The data that support the findings of this study are available upon reasonable request from the authors.

Acknowledgments

This work was supported by CNPq (302775/2018-8, 429771/2018-5, 306348/2019-5, 309537/2019-3, 440296/2021-8), Finep (442521/2019-7), CAPES (RELAII and 36788881.198744/2018-01) and FAPEMIG (TEC—RED-00282-16, APQ-02026-17, CEX-APQ-01361-14). We thank Jana Zaumseil for the access to the infrastructure at the Chair of Applied Physical Chemistry, Heidelberg.

ORCID iDs

Hudson Miranda https://orcid.org/0000-0002-9946-5224
João Luiz E Campos https://orcid.org/0000-0002-8071-0525
Cassiano Rabelo https://orcid.org/0000-0003-0488-2242
Bráulio S Archanjo https://orcid.org/0000-0001-8145-7712
Ado Jorio https://orcid.org/0000-0002-5978-2735
Luiz Gustavo Cançado https://orcid.org/0000-0003-0816-0888

References

[1] Novotny L and Hecht B 2012 *Principles of Nano-Optics* (Cambridge: Cambridge University Press)
[2] Zhang R *et al* 2013 *Nature* **498** 82–86
[3] Zhang Z, Sheng S, Wang R and Sun M 2016 *Anal. Chem.* **88** 9328–46
[4] Deckert-Gaudig T, Taguchi A, Kawata S and Deckert V 2017 *Chem. Soc. Rev.* **46** 4077–110
[5] Verma P 2017 *Chem. Rev.* **117** 6447–66
[6] Chen X, Liu P, Hu Z and Jensen L 2019 *Nat. Commun.* **10** 2567
[7] Lee J, Crampton K T, Tallarida N and Apkarian V 2019 *Nature* **568** 78–82
[8] Gadelha A C *et al* 2021 *Nature* **590** 405–9
[9] Shao F and Zenobi R 2019 *Anal. Bioanal. Chem.* **411** 37–61
[10] Meng L, Yang Z, Chen J and Sun M 2015 *Sci. Rep.* **5** 1–5
[11] Ayars E J, Hallen H D and Jahncke C L 2000 *Phys. Rev. Lett.* **85** 4180
[12] Zhang Z, Sun M, Ruan P, Zheng H and Xu H 2013 *Nanoscale* **5** 4151–5
[13] Sun M, Zhang Z, Chen L, Sheng S and Xu H 2014 *Adv. Opt. Mater.* **2** 74–80
[14] Fang Y, Zhang Z, Chen L and Sun M 2015 *Phys. Chem. Chem. Phys.* **17** 783–94
[15] Miranda H, Rabelo C, Cançado L G, Vasconcelos T L, Oliveira B S, Schulz F, Lange H, Reich S, Kusch P and Jorio A 2020 *Phys. Rev. Res.* **2** 023408
[16] Backes C *et al* 2020 *2D Mater.* **7** 022001
[17] Cançado L G, Pimenta M A, Neves B R A, Dantas M S S and Jorio A 2004 *Phys. Rev. Lett.* **93** 247401
[18] Hennighausen Z and Kar S 2021 *Electron. Struct.* **3** 014004
[19] Alden J S, Tsen A W, Huang P Y, Hovden R, Brown L, Park J, Muller D A and McEuen P L 2013 *Proc. Natl Acad. Sci.* **110** 11256–60
[20] Jorio A, Dresselhaus M S, Saito R and Dresselhaus G 2011 *Raman Spectroscopy in Graphene Related Systems* (New York: Wiley)
[21] Backes C *et al* 2019 *ACS Nano* **13** 7050–61
[22] Vasconcelos T L *et al* 2018 *Adv. Opt. Mater.* **6** 1800528
[23] Rabelo C, Miranda H, Vasconcelos T L, Cançado L G and Jorio A 2019 Tip-enhanced Raman spectroscopy of graphene *2019 4th Int. Symp. on Instrumentation Systems, Circuits and Transducers (INSCIT)* (IEEE) pp 1–6
[24] Archanjo B S, Fragneaud B, Gustavo Cançado L, Winston D, Miao F, Alberto Achete C and Medeiros-Ribeiro G 2014 *Appl. Phys. Lett.* **104** 193114
[25] Yin L J, Jiang H, Qiao J B and He L 2016 *Nat. Commun.* **7** 11760
[26] Gargiulo F and Yazyev O V 2017 *2D Mater.* **5** 015019
[27] Lin J, Fang W, Zhou W, Lupini A R, Idrobo J C, Kong J, Pennycook S J and Pantelides S T 2013 *Nano Lett.* **13** 3262–8
[28] Jiang L *et al* 2016 *Nat. Mater.* **15** 840–4
[29] Thomsen C and Reich S 2000 *Phys. Rev. Lett.* **85** 5214
[30] Beams R, Cançado L G and Novotny L 2011 *Nano Lett.* **11** 1177–81

[31] Ribeiro-Soares J et al 2015 Carbon 95 646–52
[32] Cançado L G, Da Silva M G, Ferreira E H M, Hof F, Kampioti K, Huang K, Pénicaud A, Achete C A, Capaz R B and Jorio A 2017 2D Mater. 4 025039
[33] Griffin A, Nisi K, Pepper J, Harvey A, Szydłowska B M, Coleman J N and Backes C 2020 Chem. Mater. 32 2852–62
[34] Backes C, Paton K R, Hanlon D, Yuan S, Katsnelson M I, Houston J, Smith R J, McCloskey D, Donegan J F and Coleman J N 2016 Nanoscale 8 4311–23
[35] Hassan M, Haque E, Reddy K R, Minett A I, Chen J and Gomes V G 2014 Nanoscale 6 11988–94
[36] Sarkar S, Gandla D, Venkatesh Y, Bangal P R, Ghosh S, Yang Y and Misra S 2016 Phys. Chem. Chem. Phys. 18 21278–87
[37] Kang S, Jeong Y K, Jung K H, Son Y, Choi S C, An G S, Han H and Kim K M 2019 RSC Adv. 9 38447–53
[38] Lu L, Zhu Y, Shi C and Pei Y T 2016 Carbon 109 373–83
[39] Cançado L G, Beams R, Jorio A and Novotny L 2014 Phys. Rev. X 4 031054
[40] Newville M, Stensitzki T, Allen D B, Rawlik M, Ingargiola A and Nelson A 2016 Astroph. Source Code Libr. ascl–1606
[41] Richardson W H 1972 J. Opt. Soc. Am. 62 55–59
[42] Lucy L B 1974 Astron. J. 79 745
[43] Van der Walt S, Schönberger J L, Nunez-Iglesias J, Boulogne F, Warner J D, Yager N, Gouillart E and Yu T 2014 PeerJ 2 e453
[44] Nečas D and Klapetek P 2012 Cent. Eur. J. Phys. 10 181–8
[45] Virtanen P et al 2020 Nat. Methods 17 261–72
[46] Newville M, Stensitzki T, Allen D B and Ingargiola A 2014 Lmfit: non-linear least-square minimization and curve-fitting for Python (Zenodo) (https://doi.org/10.5281/ZENODO.11813)